RSC Advances

PAPER

View Article Online
View Journal | View Issue

Cite this: *RSC Adv.*, 2022, **12**, 26934

Vitrimers trigger covalent bonded bio-silica fused composite materials for recycling, reshaping, and self-healing applications†

Salendra Sriharshitha,[a] Krishnamoorthy Krishnadevi *[ab] and Dakshinamoorthy Prasanna[c]

Received 20th June 2022
Accepted 6th September 2022

DOI: 10.1039/d2ra03794g

rsc.li/rsc-advances

In this work, a recycling, reshaping, and self-healing strategy was followed for polybenzoxazine through S–S bond cleavage reformation in vitrimers, and the supramolecular interactions are described. The E-ap benzoxazine monomer was synthesized through the Mannich condensation reaction using a renewable eugenol, 3-amino-1-propanol and paraformaldehyde. Furthermore, the E-3ap monomer was reinforced with various weight percentages (5, 10, and 15 wt%) of the thiol-ene group. Various weight percentages of functionalized bio-silica (BS) were also copolymerized with E-3ap (10%-SH) to increase the thermal stability. The structure of the monomers was confirmed by NMR and FT-IR analysis and the thermal properties of the cured materials were analyzed by DSC and TGA. Tensile test was used to study the mechanical property of the poly(E-3ap-*co*-SH)/BS material. The film was characterized by SEM and optical microscopy to investigate the self-healing properties of the poly(E-3ap-*co*-thiol-ene)/BS. Moreover, photos and video clips show the self-healing ability of a test specimen. The vitrimer-based renewable polybenzoxazine material exhibits a good recycling, reshaping, and self-healing abilities, and thus is a prime candidate for several industrial and engineering applications.

Introduction

Over the past few decades, polybenzoxazine resins have emerged as a superior class that can serve as alternatives to traditional phenolic resins because of their structural difference in the main chain.[1] They possess the characteristics of less water absorption, high glass transition temperatures (T_g) and good char yields.[2–5] Perhaps, the synthesis of benzoxazine monomers can be accomplished using any phenol, primary amine and formaldehyde or para-formaldehyde. Thus, there are a large number of possible benzoxazines after thermal curing.[6,7]

There are some limitations to the polybenzoxazines that are synthesized from eugenol, such as poor mechanical strength and rigidity.[8] However, the drawbacks of these polybenzoxazines can be overcome by designing flexible moieties that allow a huge amount of molecular diversity, controlled structures, and improved properties. For example, the cross-linking density of the resins can be increased by introducing polymerizable functionalities on benzoxazines.[9,10] The toughness and rigidity of polybenzoxazine can be manipulated using long chain amines and other soft group precursors,[11] such as hydrosilylation,[12–16] Diels–Alder,[17–20] esterification[21,22] and copolymerization.[23,24] The thermal and mechanical strength of polybenzoxazine systems can be increased by the use of filler-reinforced materials such as silica and carbon[25–27] and they have been successfully applied to obtain curable polymers bearing benzoxazines with designed properties.

Rice husk (RH) ash was a desirable material because of its high silica content (85%), high availability, low commodity cost, high specific strength and stiffness, low density (90–150 kg m^{-3}), toughness, resistance to weathering, and unique composition.[28] The RH, which was the outer covering of a rice kernel and was removed as a non-edible material, a bio-renewable and highly abundant material worldwide. RH ash was a rich source of silica, and the silica can be purified using a strong acid/base solution to remove the impurities.[29] An inorganic source of silica containing RH has been widely used in the ceramic, cement, construction, and refractory industries.[30] The incorporation of this hybrid inorganic material in benzoxazine systems will enhance their thermal stability, such as char yield.

[a]*Polymer Composites Lab, Division of Chemistry, Department of Sciences & Humanities, Vignan's Foundation for Science, Technology and Research (Deemed to Be University), Guntur, Andhra Pradesh, India. E-mail: krishchem05@gmail.com*

[b]*Department of Chemistry, Vignan Degree & PG College, Guntur, Andhra Pradesh, India*

[c]*Department of Chemistry, Vignan's Nirula Institute of Technology and Science for Women, Guntur, Andhra Pradesh, India*

† Electronic supplementary information (ESI) available: Photographic images of the prepared composites, figures of the material representing the reshaping property, EDAX elemental composition results, and optical microscopy results of poly[E-3ap-*co*-SH(15%)] and poly[E-3ap-*co*-SH(10%)]/BS_1. See https://doi.org/10.1039/d2ra03794g

Over the past two decades, the research interest was directed towards benzoxazine based smart and advanced materials rather than developing alternative materials to conventional phenolic epoxy and their composites. Similarly, polybenzoxazines have been used to produce several smart materials such as smart coatings,[11,22,23] shape memory polybenzoxazines,[31–34] super-hydrophobic surfaces,[35,36] and self-cleaning surfaces.[37,38] The occurrence of self-healing, repairing or recycling was common in nature. For example, lost or injured tissues and organs can be regenerated in most living organisms. Inspired by these spectacles, there has been great interest in studies on artificial self-healing materials over the past couple of decades.[39–42]

Based on the healing mechanism, self-healing materials were classified into two different types: intrinsic and extrinsic. The intrinsic materials can be self-healed many times under certain stimuli or even without external stimuli.[43] Yagci's research group developed a self-healing material by supramolecular interactions using poly(propyleneoxide)-based benzoxazine with varying weight ratios of acid functionalized benzoxazine.[44] The same group reported the self-healing behavior of polybenzoxazines based on metal–ligand interactions and supramolecular attraction using a polydimethylsiloxane based benzoxazine matrix.[45] The same research group also reported that benzoxazine monomers can be used as self-healing agents for a polysulfone (PSU) matrix.[46]

Among several intrinsic self-healing approaches, sulfur-containing polymer materials, namely sulfides, disulfides and trithiocarbonates were widely researched because of the easy formation of sulfur–sulfur and carbon–sulfur bonds that can be reformed when cleaved.[47] The above strategy was used to synthesize thiol-based benzoxazine chemistry and was first reported by Gorodisher *et al.*,[48] who used it to synthesize several thiol-benzoxazines.[49,50] The recycling and self-healing of commercial benzoxazine using bisphenol with dynamic sulfide linkages *via* inverse vulcanization was reported by Yagci and Kiskan *et al.*[24] Cheng *et al.*[47] reported the development of self-healing polymers from renewable material by combining thiol-ene and thiol-oxidation reactions.

To the best of our knowledge, to date, there has been no report in the literature on eco-friendly bio-based polybenzoxazines with self-healing or recycling ability with incorporated bio-silica (BS) and thiol groups (SH). We synthesized eugenol-based benzoxazine (E-3ap) with 3-amino-1-propanol and paraformaldehyde through the Mannich condensation reaction. Furthermore, we cross-linked and functionalized it with the tri-mercapto compound trimethylolpropane tris(3-mercaptopropionate), followed by incorporation of 3-MPTMS-functionalized RH silica under different weight ratios (1, 3, and 5 wt%) through thermal ring opening polymerization. The purpose of incorporation of BS was to increase the thermal stability of the prepared benzoxazine matrix and composites. Self-healing of the material was observed due to the presence of hydrogen bonds, and the recycling or repairing or reshaping was due to the presence of sulfur groups. The developed bio-based self-healing polymeric material can replace non-renewable petroleum-based phenolic resins to some extent, and can be used as a readily available material for high-performance applications.

Experimental

Materials

3-Amino-1-propanol (3-ap), trimethylolpropane-tris(3-mercaptopropionate), 3-mercaptopropyl trimethoxysilane (3-MPTMS) (99%), and dimethyldichlorosilane were procured from Sigma-Aldrich, India. Paraformaldehyde, 1,4-dioxane, ethyl acetate, anhydrous sodium sulfate (Na_2SO_4), ethanol, dichloromethane and sodium hydroxide (NaOH) were obtained from Sisco Research Laboratories (SRL), India. Eugenol was acquired from Avra Chemicals, India.

Characterization

^{1}H NMR spectra were recorded with a Bruker 400 MHz using an 8000 Hz spectral width, a relaxation delay of 3.5 s, a pulse width of 45, 32 K data points, $CDCl_3$ as the solvent, and tetramethyl silane (TMS) as an internal standard, with a minimum of 32 scans that were collected for each sample. The FT-IR spectra of bio-based benzoxazine and polybenzoxazine samples were recorded with an Agilent Cary 630 ATR spectrometer. Approximately 10 mg of sample was loaded in the ATR spectrometer, and a minimum of 16 scans was collected for each sample at a resolution of ± 4 cm^{-1}. Differential scanning calorimetry (DSC) measurements were carried out using a Hitachi DSC 7020. The instrument was calibrated with indium supplied by Hitachi and 7–10 mg of sample was used. The thermograms were recorded from RT to 300 °C under N_2 (60 ml min^{-1}) at a heating rate of 10 °C min^{-1}.

Thermogravimetric analysis (TGA) was carried out with the Hitachi STA7000 series. The instrument was calibrated with calcium oxalate and aluminum supplied by Hitachi. Approximately 10 mg of sample was analyzed under N_2 (60 ml min^{-1}) and at a heating rate of 20 °C min^{-1}. To obtain a deeper understanding of the healing behavior of the sample, it was inspected by scanning electron microscopy (SEM – VEGA3 TESCAN) and an optical microscope (Zeiss lsm 700) at different intervals of time. The mechanical/tensile tests were carried out on a computerized electronic tensile testing machine (Tensometer-2 tons).

Synthesis of eugenol (E-3ap) benzoxazine monomer

The eugenol (E-3ap) benzoxazine monomer was synthesized by mixing approximately 2 moles of paraformaldehyde with 1 mole of eugenol under vigorous stirring. Then, 1 mole of 3-amino-1-propanol was added in the presence of ethyl acetate as the solvent in a 250 ml round-bottom flask at 90 °C. The stirring was continued for 24 h until the mixture became homogeneous. The product obtained was filtered and washed three times with 2 N NaOH solution, followed by distilled water. The organic phase was dried over anhydrous Na_2SO_4, and the solvent was evaporated in a rotary evaporator. A schematic representation for the synthesis of the eugenol based benzoxazine monomer was shown in Scheme 1.

Development of the poly[E-ap-*co*-SH] composite material

A homogenous mixture of E-3ap monomer and trimethylolpropane-tris(3-mercaptopropionate) with different

weight ratios of 0, 5, 10, and 15 wt% for the poly[E-3ap], poly[E-3ap-*co*-SH(5%)], poly[E-3ap-*co*-SH(10%)], and poly[E-3ap-*co*-SH(15%)] composite materials, respectively, was prepared according to the following procedure. Approximately 5 g of synthesized E-3ap benzoxazine monomer with 2 ml of 1,4-dioxane was separately dispersed in 25 ml round bottom flasks containing magnetic pellets and stirred at room temperature for approximately 2 h. Later, varying amounts of trimethylolpropane tris(3-mercaptopropionate) were added to the above mixtures, which were stirred for approximately 40 min to obtain a homogeneous solution at room temperature. Then, the samples were thermally cured at 40 °C, 60 °C, 80 °C, 100 °C, 120 °C, 140 °C, 160 °C, 180 °C, 200 °C, and 220 °C for 1 h each and post cured at 240 °C for 1 h to obtain polybenzoxazine copolymerized thiol composites, as represented in Scheme 1 (step-I).

Fabrication of the BS incorporated poly(E-3ap-*co*-SH)/BS composite material

BS was developed and functionalized with 3-MPTMS according to our previously reported procedure.[51] The developed homogeneous solutions of the [E-3ap-*co*-SH(10%)] mixture were incorporated with different weight percentages of 1, 3, and 5 wt% of BS. Then, they were separately dispersed in 1 ml of 1,4-dioxane solvent and mixed to obtain the above solutions. The total compositions were vigorously stirred for 3 h, and then, they were separately poured onto a silane-coated glass plate and cured at 40 °C, 60 °C, 80 °C, 100 °C, 120 °C, 140 °C, 160 °C, 180 °C, 200 °C and 220 °C for 1 h each and post cured at 240 °C for 1 h to obtain poly[E-3ap-*co*-SH(10%)]/BS_1, poly[E-3ap-*co*-SH(10%)]/BS_3 and poly[E-3ap-*co*-SH(10%)]/BS_5, which were later preserved for further studies. A schematic representation for the thermal ring opening and cross-linking of poly[E-3ap-*co*-SH(10%)]/BS was shown in Scheme 1 (step-II).

Cytotoxicity – MTT assay

The HeLa human cervical cancer cell line was separately plated using 96-well plates at the concentration of 1×10^4 cells per well in minimum essential medium (MEM) with 1× antibiotic antimycotic solution and 10% fetal bovine serum (FBS, Himedia, India) in a CO_2 incubator at 37 °C with 5% CO_2. The cells were washed with 200 μl of 1× phosphate-buffered saline (PBS) and were then treated with various test concentrations of

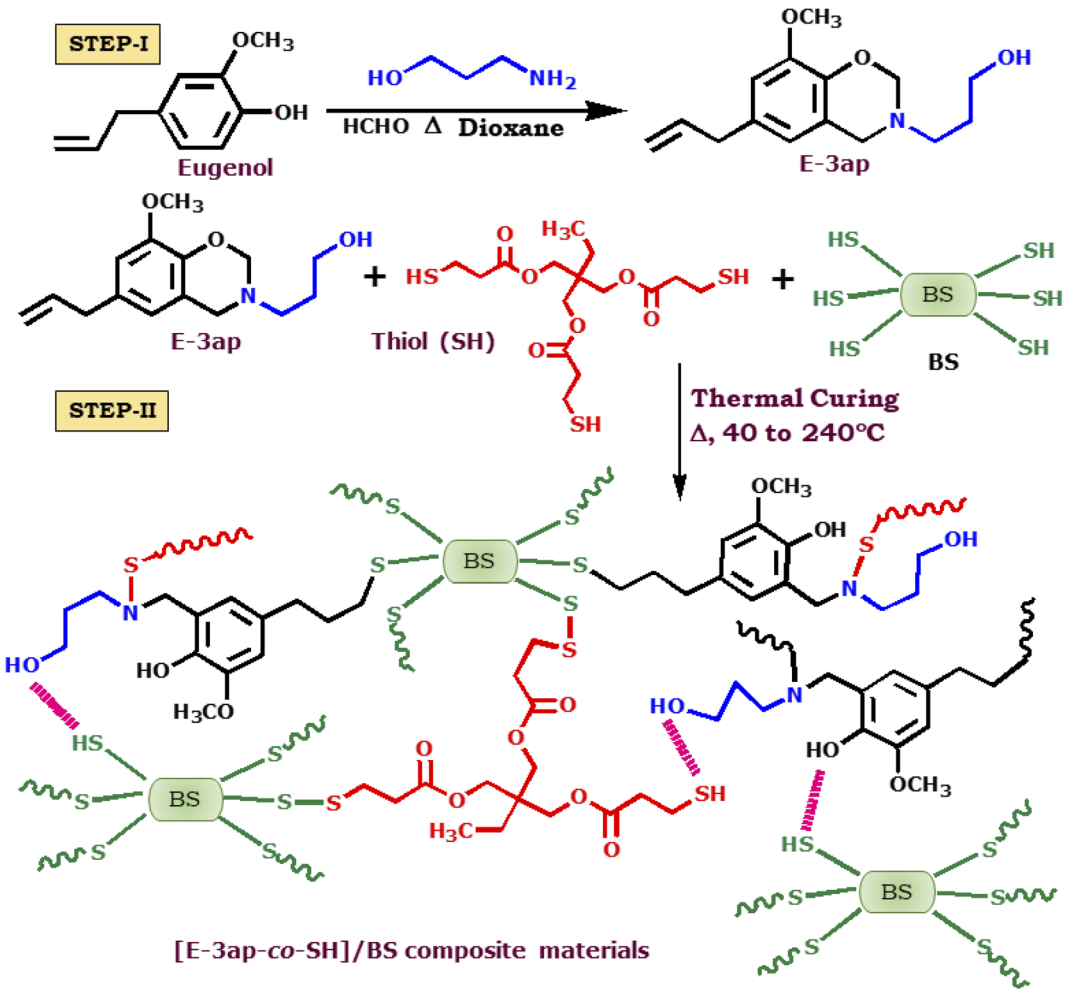

Scheme 1 Proposed schematic representation of the (step-I) synthesis of E-ap benzoxazine monomer and (step-II) thermal ring opening polymerization and cross-linking of poly[E-3ap-*co*-SH]/BS composite materials.

compound in serum-free media and incubated for 24 h. The medium was removed from the cells by aspiration at the end of the treatment period.

Next, 0.5 mg ml^{-1} MTT prepared in 1× PBS was added, and the cells were incubated at 37 °C for 4 h using a CO_2 incubator. After the incubation period, the medium containing MTT was discarded, and the cells were washed using 200 μl of PBS. The formed crystals were dissolved with 100 μl of dimethylsulfoxide (DMSO) and thoroughly mixed. The development of the purple-blue color intensity of the formazan dye was evaluated at 570 nm by the measurement of absorbance using a microplate reader.[52]

Results and discussion

Structural confirmation of the composites

The E-3ap benzoxazine monomer was successfully synthesized, and the molecular structure was confirmed using an FT-IR spectrum (Fig. 1(a)). From Fig. 1(a), the absorption peaks that appeared at 971 cm^{-1} and 1401 cm^{-1} represent the oxazine moiety attached to the benzene ring. Similarly, the vibrational peaks that appeared at 1216 cm^{-1}, 1152 cm^{-1} and 1085 cm^{-1} represent the C–O–C stretching vibrations. Aliphatic stretching vibrations were observed at 2950 cm^{-1} and 2840 cm^{-1}. The peak at 3467 cm^{-1} confirms the presence of the –OH group in the E-3ap benzoxazine monomer.

Furthermore, the FT-IR spectra of the neat (E-3ap cured sample) and poly(E-3ap-*co*-SH)/BS materials were studied from Fig. 1(b) and (c) explains the structural characteristic spectrum of the neat sample. The absorption of the vibrational peak disappeared at 973 cm^{-1}, which confirms the ring opening of benzoxazine and also shows the spectrum of poly(E-3ap-*co*-SH) BS with E-3ap, 10% of tri-mercapto compound and differing percentages (1, 3, and 5%) of BS. The appearance of peaks at 1065 cm^{-1} corresponds to Si–O–C, the peaks at 1150 cm^{-1} show C–O, and at 1213 cm^{-1} represents the Si–C bending vibrational peaks of the tri-mercapto compound and BS. The peaks at 3385 cm^{-1} show the –OH bridging groups present in the structure.

Curing behaviour of the E-3ap monomer

The curing behaviour of the synthesized E-3ap monomer was characterized by DSC analysis, and is shown in Fig. 1(d). From the DSC thermogram, the exothermic peak appeared at 260 °C and confirmed the ring opening polymerization temperature of the E-3ap benzoxazine monomer. Generally, the exothermic

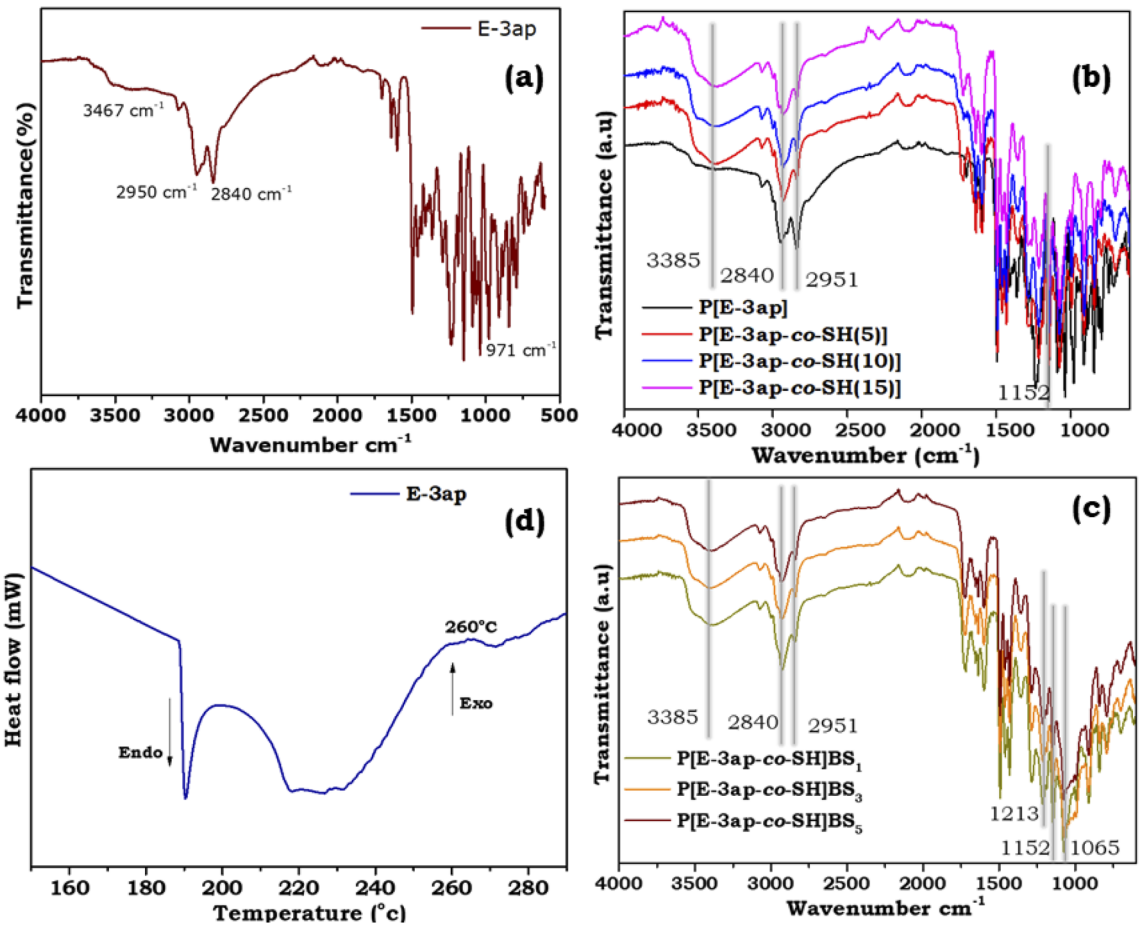

Fig. 1 The FT-IR spectrum of (a) E-3ap benzoxazine monomer, (b) cured E-3ap and poly[E-3ap-*co*-SH], (c) poly(E-3ap-*co*-SH)/BS composites and (d) DSC thermogram of the E-3ap benzoxazine monomer.

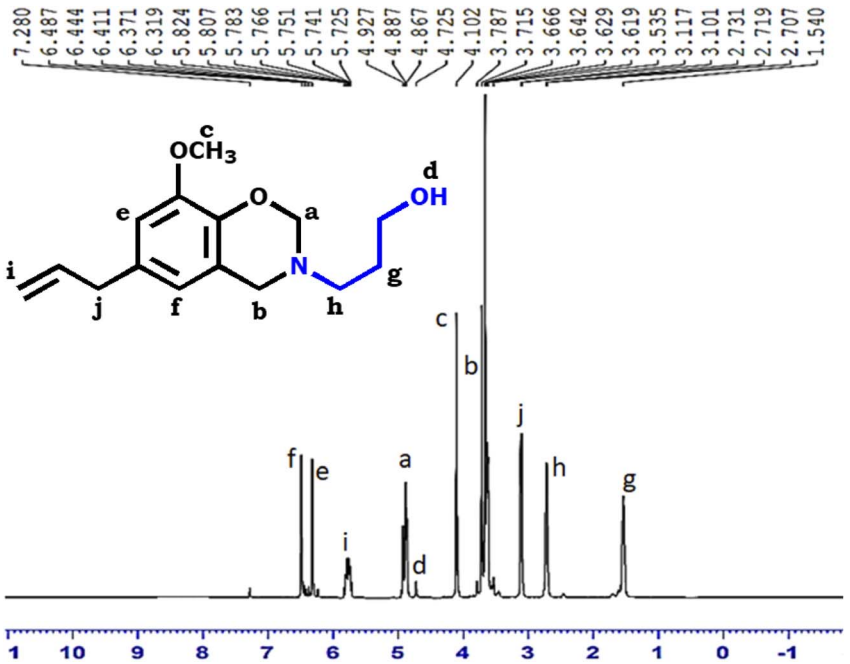

Fig. 2 ^{1}H NMR spectrum of the E-3ap benzoxazine monomer.

peak describes the curing temperature of the benzoxazine. From the graph, the initial temperature (T_i), the peak temperature (T_p), and the final temperature (T_f) were observed at 240 °C, 260 °C, and 270 °C, respectively, which confirm the complete polymerization of the benzoxazine monomer to highly cross-linked polybenzoxazine through phenolic Mannich bridges. From all the above studies, Fig. 1(a)–(d) confirmed the structural as well as the curing temperature of the synthesised E-3ap monomer and the polymers with different weight ratios of SH and BS.

^{1}H NMR spectrum of the E-3ap monomer

The structure of E-3ap was further demonstrated using ^{1}H NMR spectra. Fig. 2 shows the ^{1}H NMR spectrum of E-3ap and the characteristic signals of oxazine protons in Ph–CH_2–N and O–CH_2–N were observed at 3.7 ppm and 4.8 ppm, respectively. The –OH of the amino-propanol appeared at 4.8 ppm. The aromatic proton signals appeared in the range between 6.3 and 6.7 ppm. The –CH_3 signal of eugenol (methyl) appeared at 4.1 ppm.

Thermal properties

The thermal behaviour of the E-3ap neat sample and various percentages of thiol incorporated poly(E-3ap-*co*-SH) followed by various percentages of BS integrated poly(E-3ap-*co*-SH)/BS materials were studied using DSC and TGA (Fig. 3 and 4). Fig. 3 illustrates the DSC spectrum of the neat, poly(E-3ap-*co*-SH), and poly(E-3ap-*co*-SH)/BS materials, which signifies the glass transition temperature (T_g) of the developed benzoxazine composites. The T_g values increased after increasing the percentage of thiol and BS into the benzoxazine composites. The T_g values were 123 °C, 132 °C, 133 °C, 140 °C, 150 °C, 160 °C and 167 °C for poly(E-3ap), poly(E-3ap-*co*-SH(5)), poly(E-3ap-*co*-SH(10)), poly(E-3ap-*co*-SH(15)), poly(E-3ap-*co*-SH)/BS_1, poly(E-3ap-*co*-SH)/BS_3, and poly(E-3ap-*co*-SH)/BS_5, respectively. The values were enhanced due to the presence of S–S vitrimer linkages for the covalent bond formation through supramolecular interaction and cross-linking network structures that allowed free mobility of the molecules.

The thermal stability and degradation characteristics of poly[E-3ap], poly[E-3ap-*co*-SH(5%)], poly[E-3ap-*co*-SH(10%)], poly[E-3ap-*co*-SH(15%)], and hybrid materials of poly[E-3ap-*co*-SH(10%)]/BS_1, poly[E-3ap-*co*-SH(10%)]/BS_3, and poly[E-3ap-*co*-

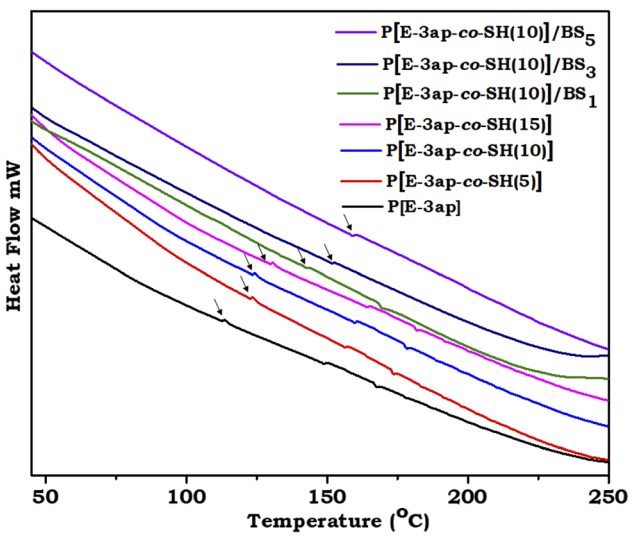

Fig. 3 DSC thermogram of cured E-3ap, as well as the poly[E-3ap-*co*-SH] and poly(E-3ap-*co*-SH)/BS composites.

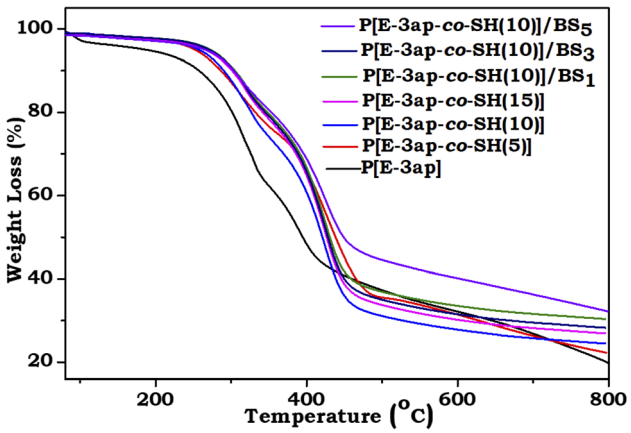

Fig. 4 TGA analysis of poly(E-3ap-*co*-SH)/BS composites.

Table 1 Thermal properties and char yield of bio-based polybenzoxazines

Composites	Weight loss at temperature (°C)			Char yield % at 800 °C
	5 wt%	10 wt%	Max. wt%	
Poly[E-3-ap]	185	257	450	19
Poly[E-3ap-*co*-SH(5%)]	277	306	444	22
Poly[E-3ap-*co*-SH(10%)]	256	288	463	24
Poly[E-3ap-*co*-SH(15%)]	261	291	437	27
Poly[E-3ap-*co*-SH(10%)]/BS_1	273	300	442	28
Poly[E-3ap-*co*-SH(10%)]/BS_3	260	292	445	30
Poly[E-3ap-*co*-SH(10%)]/BS_5	279	308	497	34

SH(10%)]/BS_5 bio-based composites were determined using TGA analysis under a nitrogen atmosphere and the obtained results are shown in Fig. 4. The degradation behavior of hybrid bio-based composites at 5% weight (T^d 5%), 10% weight (T^d 10%) and maximum degradation (T^d max) are listed in Table 1. The maximum degradation temperature was observed to be 450 °C, 444 °C, 463 °C, 437 °C, 442 °C, 445 °C and 497 °C for poly[E-3ap], poly[E-3ap-*co*-SH(5%)], poly[E-3ap-*co*-SH(10%)], and poly[E-3ap-*co*-SH(15%)] material, respectively. Similarly, the maximum degradation temperature (T^d max) of poly[E-3ap-*co*-SH(10%)]/BS_1, poly[E-3ap-*co*-SH(10%)]/BS_3, and poly[E-3ap-*co*-SH(10%)]/BS_5 was 442 °C, 445 °C and 497 °C, respectively. The char yield values from the thermogram for poly[E-3ap], poly[E-3ap-*co*-SH(5%)], poly[E-3ap-*co*-SH(10%)], poly[E-3ap-*co*-SH(15%)] and hybrid materials of poly[E-3ap-*co*-SH(10%)]/BS_1, poly[E-3ap-*co*-SH(10%)]/BS_3, and poly[E-3ap-*co*-SH(10%)]/BS_5 bio-based composites were 19, 22, 24, 27, 28, 30, and 33, respectively (Table 1). The char yield values increased with the percentage of sulphur (S) and silica (Si) in the poly[E-3ap] composites. Among all the 5 wt%-loaded RH ash samples of the poly[E-3ap-*co*-SH(10%)]/BS_5 composite material, there was a stronger thermal stability as compared to the neat E-3ap matrix and other hybrid composites, and this might be due to the development of a network complex structure in the system. Furthermore, the incorporation of BS in the benzoxazine matrix will lower the degradation of volatiles and form a protective passive silica layer on the surface of the prepared benzoxazine composites to prevent the oxidation of the interior part of the matrix.[51]

Self-healing, recycling, and reshaping behaviour of the cured materials

The recyclability, reshaping, and self-healing of the poly[E-3ap-*co*-SH] and poly[E-3ap-*co*-SH]/BS_1 composites were studied for the cured films, as shown in Fig. 5. The prepared polymer samples were cut into tiny pieces with scissors and then, the cut pieces were transferred onto a Teflon sheet. The sheet with damaged pieces of poly[E-3ap-*co*-SH]/BS sample was molded and clipped. Here, we used a medium-sized paper binder clamp to confirm the reshaping and self-healing of the material. The pressure of the binder clamp was adequate to assist the samples in regaining their shape. The recyclability, reshaping, and self-healing of the materials were performed at room temperature without applying any external heat for reformation of the samples and the damaged pieces regained their original shape within 10 h.

The poly[E-3ap-*co*-SH]/BS materials with different weight ratios of 1, 3 and 5% BS were tested, and all the composites exhibited satisfactory recyclability, reshaping and self-healing because of the existence of hydrogen bonding interactions between phenolic –OH and the thiol group (SH) and also due to the presence of S–S covalent bonds along with the nature of the vitrimer linkage in the structure. The sulfur group formed weak S–S (disulfide) and C–S linkages derived from thiol-ene, functionalized BS and the long allyl chain of the eugenol, and it is likely that these weaker interactions will undergo bond deformation and reformation.[47] This bond breaking and making was confirmed using FTIR spectra (see Fig. 3). The phenomenon peak at 2363 cm^{-1} indicates the S–H group of thiol-ene and after the incorporation of BS in various weight ratios, the peak completely disappeared. This showed that the prepared polymer matrix of the poly[E-3ap-*co*-SH(5)], poly[E-3ap-*co*-SH(10)], poly[E-3ap-*co*-SH(15)], and poly[E-3ap-*co*-SH(10)]/BS materials was undergoing the above recyclability, reshaping, and self-healing activities (Fig. 5).

Shape memory

Shape memory or shape memory effect (SME) was the process by which material in a deformed state (temporary shape) was restored to its original state (permanent shape).[53] The SME in polybenzoxazine was generally temperature stimulated and therefore the deformation process takes place at a certain temperature.[54,55] The advantage of developed poly[E-3ap-*co*-SH(10%)] material exhibits SME without any external stimulation such as temperature. The SME occurs because of the flexibility of the sample that occurs due to the presence of weak disulfide S–S and C–S linkages in the existing vitrimer structure. The shape memory process of poly[E-3ap-*co*-SH(10%)] was examined, and photographs are presented in Fig. S1 and S2.† The polymer material exhibited multiple SMEs at room

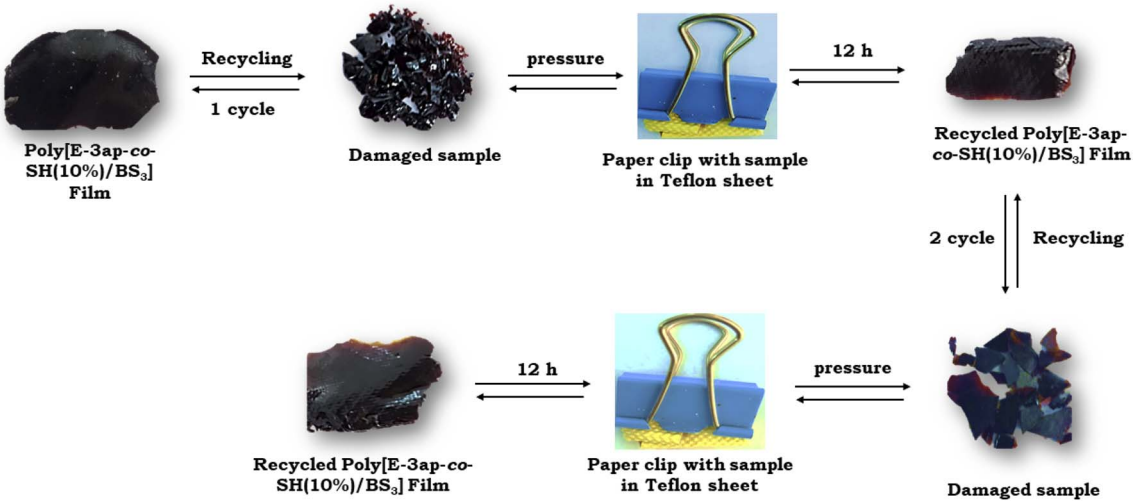

Fig. 5 Photographs of the prepared poly[E-3ap-*co*-SH(10)]BS composites showing their ability to recycle after damage.

temperature without any external provocation, and with a recovery time interval of 10 s.

Scanning electron microscopy

The compatibility and surface morphology of neat E-3ap and various percentages of BS-fused poly(E-3ap-*co*-SH)/BS composites were examined by SEM and were shown in Fig. 6. Fig. 6(a) shows the surface morphology of neat poly[E-3ap], which exhibits a smooth surface with a non-phase-separated homogeneous morphology that confirms the crosslinking reaction between benzoxazine and thiol (SH) groups. Fig. 6(b)–(d) confirms the successful integration of thiol-functionalized

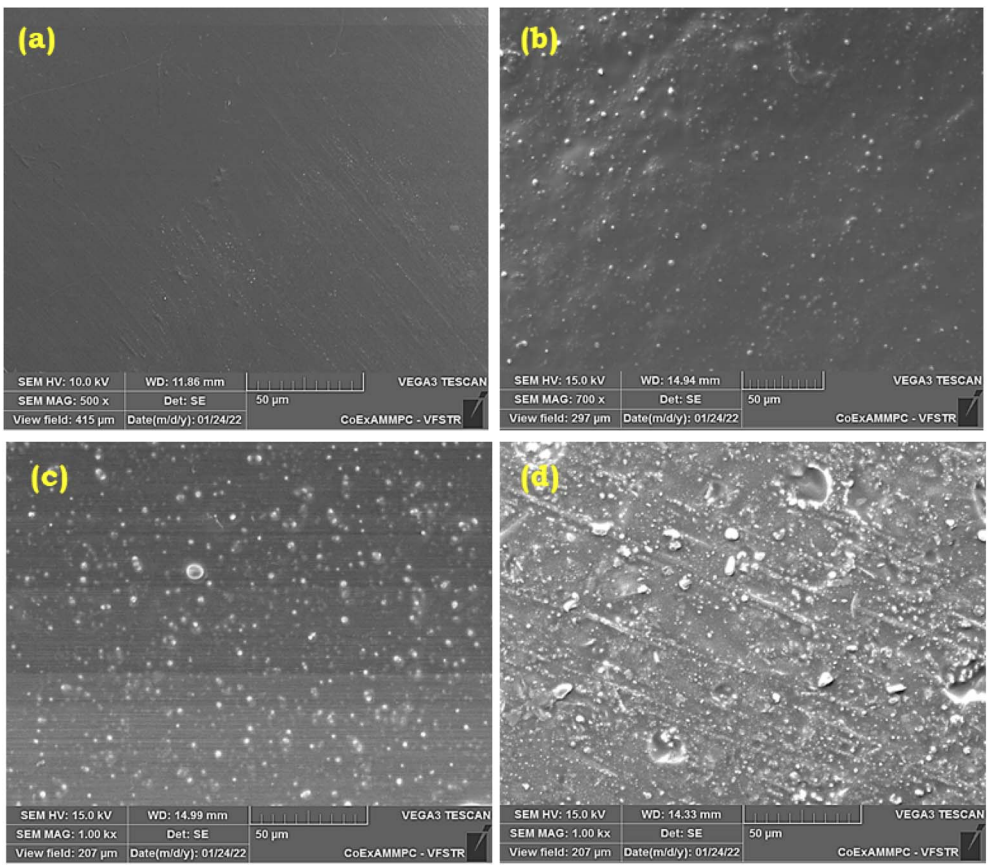

Fig. 6 SEM images of (a) poly[E-3ap] neat, (b) poly[E-3ap-*co*-SH(10%)]/BS_1, (c) poly[E-3ap-*co*-SH(10%)]/BS_3, and (d) poly[E-3ap-*co*-SH(10%)]/BS_5.

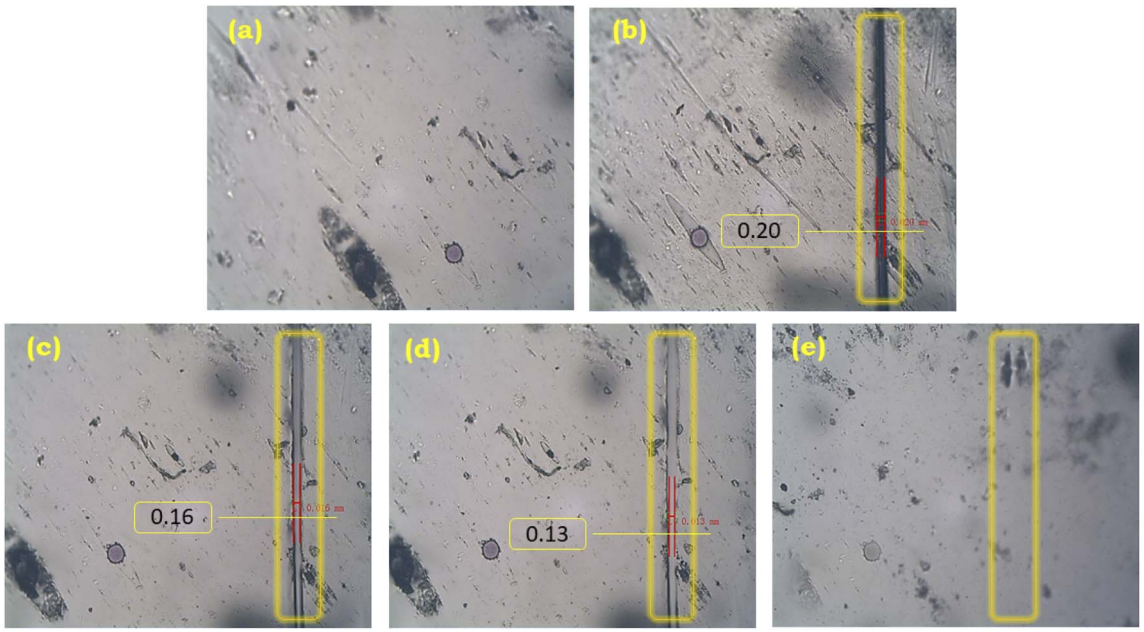

Fig. 7 Optical microscopy images of poly[E-3ap-*co*-SH(10%)]: (a) neat, (b) damaged, (c) after 2 h, (d) after 3 h, and (e) after 10 h.

BS into the composites. Fig. 6(b) to (d) shows that the smoothness of the surface has deteriorated due to the addition of BS, and that non-phase separation occurred, as well as the uniform dispersion of BS throughout the poly(E-3ap-*co*-SH)/BS matrix due to the crosslinking reaction among benzoxazine, thiol groups and BS units through thiol-ene and S–S vitrimer bond formation. Fig. S3 and Table S1† reveal the results of elemental mapping and elemental composition data from SEM analysis and confirm the occurrence of silica in the composites.

Optical microscopy

The process of self-healing was studied at room temperature at various time intervals, and then the entire healing process was verified through an optical microscope for the poly[E-3ap-*co*-SH(10%)], poly[E-3ap-*co*-SH(15%)], and poly[E-3ap-*co*-SH(10%)]/BS_1 samples. Fig. 7 shows an optical microscope image of the poly[E-3ap-*co*-SH(10%)] sample at different healing times and Fig. S4 and S5† show optical images of the poly[E-3ap-*co*-SH(15%)] and poly[E-3ap-*co*-SH(10%)]/BS_1 samples, respectively. The width of the damaged surface for poly[E-3ap-*co*-SH(10%)] was initially 0.020 mm, and after 2 h and 3 h of healing, it was observed that the width decreased to 0.016 mm and 0.013 mm, respectively. Finally, after 10 h of time, the damaged surface had been completely healed and turned into the original surface. The healing process occurred due to the vitrimer covalent bond formation in the S–S bond and occurrence of hydrogen bonds between the –SH (thiol) unit and –OH group present in the benzoxazine unit. Similarly, for poly[E-3ap-*co*-SH(15%)] (Fig. S4†), the width was initially 0.040 mm, and after 2 h and 3 h of healing, the width decreased to 0.033 mm and 0.014 mm, respectively. Finally, after 6 h, we observed the complete healing of the material.

The complete healing process for poly[E-3ap-*co*-SH(10%)] was slower than that of the poly[E-3ap-*co*-SH(15%)] material because of the increased percentage of soft units of the SH (thiol) group. Moreover, for poly[E-3ap-*co*-SH(10%)]/BS_1, the healing process required a longer amount of time than the two above mentioned samples. The initial width for poly[E-3ap-*co*-SH(10%)]/BS_1 (Fig. S5†) was 0.026 mm, which decreased to 0.019 mm after 2 h. After 24 h, there was complete healing of the material because of the incorporation of silica-containing hybrid hard BS material. The entire process of the damage and healing was performed on the surfaces of the materials without applying any external pressure.

Mechanical/tensile tests of the poly(E-3ap-*co*-SH)/BS composites

Mechanical studies supported the self-healing properties of the prepared vitrimers of covalent bonded bio-based material through tensile tests. Fig. 8 shows the results for the poly[Ea-3p-*co*-SH(10%)], poly[E-3ap-*co*-SH(15%)], poly[E-3ap-*co*-SH(10%)]/BS_1, poly[E-3ap-*co*-SH(10%)]/BS_3, and poly[E-3ap-*co*-SH(10%)]/BS_5 samples and the tensile strength values were 40 MPa, 36 MPa, 35 MPa, 32 MPa, and 29 MPa, respectively, while the strain was observed to be approximately 70% for the prepared polymer composites. The poly[Ea-3p-*co*-SH(10%)] and poly[E-3ap-*co*-SH(15%)] materials showed slightly higher strength values compared with the poly[Ea-3p-*co*-SH(10%)$BS_{1,3,5}$] composites because of the hydrogen bonding interactions between the prepared benzoxazine and the thiol-ene (SH) (Scheme 1-step II), in which the flexibility in the designed structure was increased. Furthermore, upon increasing the weight ratio percentages of BS, the elasticity and flexibility of the composites decreased, and the toughness increased (Table 2). This occurred due to the presence of silica hybrid material

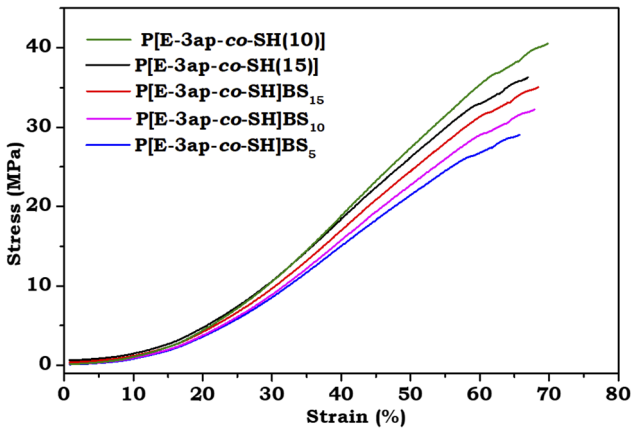

Fig. 8 Tensile test results for poly[E-3ap-*co*-SH(10%)], poly[E-3ap-*co*-SH(15%)], poly[E-3ap-*co*-SH(10%)]/BS_1, poly[E-3ap-*co*-SH(10%)]/BS_3, and poly[E-3ap-*co*-SH(10%)]/BS_5, showing the stress–strain curves.

forming additional crosslinking networks among the polybenzoxazine, thiol-ene (SH), and BS groups, which feature the formation of weak S–S and C–S linkages in the vitrimer structure.

Cytotoxicity test

The prepared monomer of E-3ap was tested to investigate its biological activity or biocompatibility using the MTT assay method to determine the *in vitro* cytotoxicity. Cell viability and cytotoxicity was determined for E-3ap, which was used as a substrate for HeLa cells. Live HeLa cells were incubated with various concentrations of E-3ap (control, and 25 to 500 μg ml^{-1}) for 24 h and then the percentage of cell viability was determined by the standard MTT method. The percentage of cell viability decreased with increasing concentration of E-3ap. The half maximal inhibitory concentration (IC_{50}) for E-3ap was 125.1 ± 2.07 μg ml^{-1}. The cell viability for 25, 50, 100, 250, and 500 μg ml^{-1} of E-3ap were valued to be 94.26%, 90.99%, 62.60%, 15.79% and 5.82%, respectively and for the control 99.92%. The results were illustrated in Fig. 9, 10 and Table 3, which show that E-3ap exhibited negligible cytotoxicity at the 500 and 250 μg ml^{-1} concentrations. After increasing the concentration of E-3ap from 100 to 250 μg ml^{-1}, the percentage of cell viability slightly increased. The absorbance (OD) was measured at 570 nm for HeLa cells on E-3ap monomers. Hence, E-3ap was selected as the more optimal substrate for culture with the HeLa cells and exhibited less cytotoxicity and increased percentage of cell viability when compared with previous studies.[56,57]

Table 2 Recycling, elasticity/flexibility, and self-healing nature of bio-based polybenzoxazines

Sample	Thiol-ene (SH) (%)	Bio-silica (BS) (%)	Recycling	Elasticity/flexibility/brittleness	Self-healing
E-3ap	—	—	—	Highly brittle	—
E-3ap	5	—	Yes	Less brittle	Yes
	10	—	Yes	Highly elastic	Yes
	15	—	Yes	Very highly elastic	Yes
E-3ap	10	1	Yes	Elastic	Yes
	10	3	Yes	Less elastic	Yes
	10	5	Yes	Very less elastic	Yes

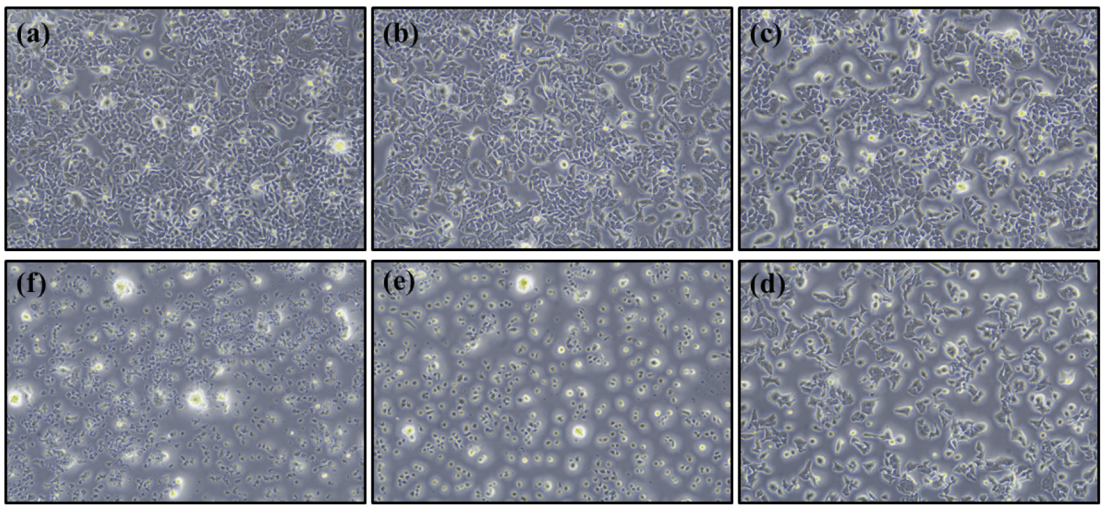

Fig. 9 *In vitro* cytotoxicity tests using the MTT assay for staining of HeLa cells treated with (a) control, (b) 25 μg ml^{-1}, (c) 50 μg ml^{-1}, (d) 100 μg ml^{-1}, (e) 250 μg ml^{-1}, and (f) 500 μg ml^{-1} of E-3ap.

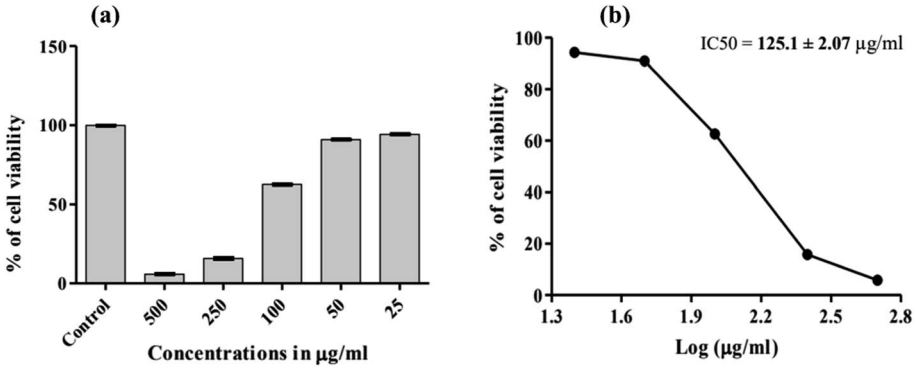

Fig. 10 Tests with the E-3ap monomer to determine % cell viability for the control, different concentrations and inhibitory concentrations (IC_{50}).

Table 3 Percentage of cell viability values at different concentrations

Concentration (µg ml^{-1})	Cell viability (%)			Mean	Standard deviation	Standard error
500	4.78	5.98	6.70	5.82	0.97	0.56
250	14.35	16.03	16.99	15.79	1.33	0.77
100	61.72	62.68	63.40	62.60	0.84	0.49
50	90.19	91.87	90.91	90.99	0.84	0.49
25	93.30	94.50	94.98	94.26	0.86	0.50
Control	100.72	99.28	99.76	99.92	0.73	0.42

Conclusion

In this work, we developed bio-based, eco-friendly poly(E-3ap-*co*-SH)/BS, which were vitrimers with excellent self-healing, recycling and reshaping properties. Upon incorporation of varying percentages of BS, the char yield % was increased and there was also satisfactory thermal stability, which was studied using TGA. The self-healing abilities were demonstrated by optical microscope and scanning electron microscope and confirm the uniform distribution of BS and the effective self-healing of damaged films at different time intervals. The mechanical properties as determined by the tensile test also evidenced that the composite films possessed shape memory and self-healing properties based on the flexible nature of the composite materials. Overall, the synthesized vitrimers with varying percentages of SH and BS demonstrated satisfactory recycling, reshaping, and self-healing properties because of the strong hydrogen bonding interactions and S–S bond cleavage and linkages at room temperature without applying any pressure. The cytotoxicity for the synthesised monomer was negligible at low concentrations and thus this bio-material possesses the potential to be used for high performance applications.

Conflicts of interest

There are no conflicts to declare.

Acknowledgements

We wish to thank VFSTR for their research facilities; CoEx-AMMPC for the FT-IR, DSC, TGA, SEM, and optical microscopy characterizations; and the VIT for the ^{1}H NMR characterization.

References

1 B. Kiskan, N. N. Ghosh and Y. Yagci, *Polym. Int.*, 2010, **60**(2), 167–177.
2 B. Lochab, S. Shukla and I. K. Varma, *RSC Adv.*, 2014, **4**, 21712–21752.
3 H. Ishida and T. Agag, *Handbook of Benzoxazine Resins*, Elsevier, Amsterdam, 2011, pp. 355–362.
4 K. Chiou and H. Ishida, *Curr. Org. Chem.*, 2013, **17**, 913–925.
5 Y. X. Wang and H. Ishida, *Polymer*, 1999, **40**, 4563–4570.
6 A. Chernykh, T. Agag and H. Ishida, *Macromolecules*, 2009, **42**, 5121–5127.
7 N. N. Ghosh, B. Kiskan and Y. Yagci, *Prog. Polym. Sci.*, 2007, **32**, 1344–1391.
8 P. Thirukumaran, A. Shakilaparveen and M. Sarojadevi, *Advanced and Emerging Polybenzoxazine Science and Technology*, Elsevier, 2017, ch. 27, pp. 523–531.
9 A. Divambal, A. Nagarjuna and L. Bimlesh, *Front. Chem.*, 2020, **8**, 2296–2646.
10 H. Yao, X. Lu, Z. Xin, X. Li, C. Chen and Y. Cao, *Colloids Surf., A*, 2021, **616**, 26209.
11 S. Sriharshitha, K. Krishnadevi, S. Devaraju, V. Srinivasadesikan and S. L. Lee, *ACS Omega*, 2020, **5**(51), 33178–33185.
12 S. Devaraju, K. Krishnadevi, S. Sriharshitha and M. Alagar, *J. Polym. Environ.*, 2019, **27**, 141–147.
13 M. Selvi, M. R. Vengatesan, S. Devaraju, M. Kumar and M. Alagar, *RSC Adv.*, 2014, **4**, 8446.

14 R. Yang, B. Hao, L. Sun and K. Zhang, *J. Appl. Polym. Sci.*, 2021, **138**(6), 49792.
15 B. Kiskan, B. Aydogan and Y. Yagci, *J. Polym. Sci., Part A: Polym. Chem.*, 2009, **47**, 804–811.
16 Y.-J. Lee, S.-W. Kuo, C.-F. Huang and F.-C. Chang, *Polymer*, 2006, **47**(12), 4378–4386.
17 Z. Strin, A. Rucigaj and M. Krajnc, *eXPRESS Polym. Lett.*, 2016, **10**(7), 537–547.
18 Ž. Stirn, A. Ručigaj, J. Karger-Kocsis and M. Krajnc, *Macromol. Mater. Eng.*, 2018, **303**(10), 1800284.
19 Y. Cao, J. Zhang, D. Zhang, Y. Lv, J. Li, Y. Xu, K. He, G. Chen, C. Yuan, B. Zeng and L. Dai, *J. Mater. Sci.*, 2020, **55**, 11325–11338.
20 S. Schäfer and G. Kickelbick, *ACS Appl. Nano Mater.*, 2018, **1**(6), 2640–2652.
21 C. P. R. Nair, *Prog. Polym. Sci.*, 2004, **29**, 401–498.
22 F. Fu, M. Huang, W. Zhang, Y. Zhao and X. Liu, *Sci. Rep.*, 2018, **8**, 10325.
23 B. Satheesh Kumar and K. S. Santhosh Kumar, *Handbook of Thermoset Plastics*, William Andrew Publishing, 4th edn, 2022, ch. 3, pp. 41–64.
24 M. Arslan, B. Kiskan and Y. Yagci, *Sci. Rep.*, 2017, **7**, 5207.
25 A. Hariharan, K. Srinivasan, C. Murthy and M. Alagar, *New J. Chem.*, 2018, **42**, 4067–4080.
26 K. Krishnadevi, S. Devaraju, E. Naveena and M. Alagar, *Polym. Adv. Technol.*, 2019, **30**, 1856–1864.
27 L. Dumas, L. Bonnaud, M. Olivier, M. Poorteman and P. Dubois, *Eur. Polym. J.*, 2015, **67**, 494–502.
28 K. Krishnadevi and V. Selvaraj, *New J. Chem.*, 2015, **39**, 6555–6567.
29 U. Kalapathy, A. Proctor and J. Shultz, *Bioresour. Technol.*, 2000, **73**(3), 257–262.
30 K. Krishnadevi and V. Selvaraj, *Polym. Bull.*, 2017, **74**, 1791–1815.
31 S. Zhang, Q. Ran, Q. Fu and Y. Gu, *Macromolecules*, 2018, **51**(17), 6561–6570.
32 Y. Liu, S. Song, X. Su, A. Wang, S. Shen and C. Li, *J. Appl. Polym. Sci.*, 2017, **134**, 45443.
33 P. Mora, H. Schäfer, C. Jubsilp, S. Rimdusit and K. Koschek, *Chem.–Asian J.*, 2019, **14**, 4129.
34 N. Erden and S. C. Jana, *Macromol. Chem. Phys.*, 2013, **214**, 1225–1237.
35 X. Cao, J. Pan, G. Cai, S. Xiao, X. Ma, X. Zhang and Z. Dong, *Prog. Org. Coat.*, 2022, **163**, 106630.
36 Y. Cao, C. Chen, X. Lu, D. Xu, J. Huang and Z. Xin, *Surf. Coat. Technol.*, 2021, **405**, 126569.
37 H. Zhang, X. Lu, Z. Xin, W. Zhang and C. Zhou, *Prog. Org. Coat.*, 2018, **123**, 254–260.
38 H. Yao, X. Lu, Z. Xin, H. Zhang and X. Li, *Sep. Purif. Technol.*, 2019, **229**, 115792.
39 Z. Wei, J. H. Yang, J. X. Zhou, F. Xu, M. Zrínyi, P. H. Dussault, Y. Osadag and Y. M. Chen, *Chem. Soc. Rev.*, 2014, **43**, 8114–8131.
40 S. J. Benight, C. Wang, J. B. H. Tok and Z. N. Bao, *Prog. Polym. Sci.*, 2013, **38**, 1961–1977.
41 S. Billiet, X. K. D. Hillewaere, R. F. A. Teixeira and F. E. Du Prez, *Macromol. Rapid Commun.*, 2013, **34**, 290–309.
42 L. T. T. Nguyen, H. T. Nguyen and T. T. Truong, *J. Polym. Res.*, 2015, **22**, 186.
43 N. K. Guimard, K. K. Oehlenschlaeger, J. W. Zhou, S. Hilf, F. G. Schmidt and C. Barner-Kowollik, *Macromol. Chem. Phys.*, 2012, **213**, 131–143.
44 M. Arslan, B. Kiskan and Y. Yagci, *Macromolecules*, 2015, **48**, 1329–1334.
45 M. Arslan, B. Kiskan and Y. Yagci, *Macromolecules*, 2018, **51**, 10095–10103.
46 O. S. Taskin, B. Kiskan and Y. Yagci, *Macromolecules*, 2013, **46**, 8773–8778.
47 C. Cheng, X. Zhang, X. Chen, J. Li, Q. Huang, Z. Hu and Y. Tu, *J. Polym. Res.*, 2016, **23**, 110.
48 I. Gorodisher, R. J. DeVoe and R. J. Webb, *Handbook of Benzoxazine Resins*, Elsevier, 2011, ch. 11, pp. 211–234.
49 L. Yu, L. H. Wang, Z. T. Hu, Y. Z. You, D. C. Wu and C. Y. Hong, *Polym. Chem.*, 2015, **6**, 1527–1532.
50 N. Zaquen, B. Wenn, K. Ranieri, J. Vandenbergh and T. Junkers, *J. Polym. Sci., Part A: Polym. Chem.*, 2014, **52**, 178–187.
51 K. Krishnadevi, S. Devaraju, S. Sriharshitha, M. Alagar and Y. Keerthi Priya, *Polym. Bull.*, 2020, **77**, 2501–2520.
52 L. Florento, R. Matias, E. Tuaño, K. Santiago, F. Dela Cruz and A. Tuazon, *Int. J. Biomed. Sci.*, 2012, **8**(1), 76–80.
53 L. Yan, J. Lou, J. Yuan and J. Deng, *RSC Adv.*, 2021, **11**, 28838–28850.
54 K. Gall, M. L. Dunn, Y. P. Liu, D. Finch, M. Lake and N. A. Munshi, *Acta Mater.*, 2002, **50**, 5115–5126.
55 K. Gall, C. M. Yakacki, Y. Liu, R. Shandas, N. Willett and K. S. Anseth, *J. Biomed. Mater. Res., Part A*, 2005, **73**, 339–348.
56 Y. Zuo, Y. Zhang, T. Yang, Z. Gou and W. Lin, *New J. Chem.*, 2018, **42**, 14281–14289.
57 Z. Wang, S. Yao, K. Song, X. Gong, S. Zhang, S. Gao and Z. Lu, *Green Chem.*, 2020, **22**, 3481–3488.